Intercellular Communication Controls Agonist-Induced Calcium Oscillations Independently of Gap Junctions in Smooth Muscle Cells.

Authors

Suzanne E Stasiak[1], Ryan R Jamieson[1], Jeff Bouffard[1,2], Erin .J. Cram[2,1] and Harikrishnan Parameswaran[1*]

Affiliations

[1] Department of Bioengineering, Northeastern University, Boston, MA 02115.

[2] Department of Biology, Northeastern University, Boston, MA 02115.

*Correspondence may be addressed to h.parameswaran@northeastern.edu.

Abstract

In this study, we report the existence of a communication system among human smooth muscle cells that uses mechanical forces to frequency modulate long-range calcium waves. An important consequence of this mechanical signaling is that changes in stiffness of the underlying extracellular matrix can interfere with the frequency modulation of Ca^{2+} waves causing smooth muscle cells from healthy human donors to falsely perceive a much higher agonist dose than they actually received. This aberrant sensing of contractile agonist dose on stiffer matrices is completely absent in isolated smooth muscle cells, even though the isolated cells can sense matrix rigidity. We show that the intercellular communication that enables this collective Ca^{2+} response in smooth muscle cells does not involve transport across gap junctions or extracellular diffusion of signaling molecules. Instead, our data support a collective model in which mechanical signaling among smooth muscle cells regulates their response to contractile agonists.

Introduction

Excessive constriction of hollow, tubular transport organs including the airways and the vasculature is a common pathophysiological feature of widespread diseases like asthma and hypertension. The vessel/airway wall undergoes significant pathological changes in the smooth muscle and in the extracellular matrix (ECM) that surrounds and supports the cells with the onset of disease (*1*, *2*). The search for mechanisms that underlie the development of these diseases and the search for novel therapies has largely focused on the smooth muscle cells (SMCs), as they are the primary effectors of constriction (*3*). Pathological changes in the ECM, on the other hand, have not received much attention (*1*, *4*). More recent studies show that changes in the ECM can impact organ function at the very early stages, and can even precede the thickening of the muscle layer (*5*). Perhaps, mechanobiological interactions between healthy SMCs and an altered ECM are playing a more critical role in the pathogenesis and progression of diseases like asthma and hypertension than is currently appreciated. In this study, we examined how changes in the matrix stiffness can impact how SMCs sense the dose of an applied agonist.

Agonist-induced Ca^{2+} oscillations and long-range Ca^{2+} waves are critical mechanisms that regulate vital parameters such as blood pressure and airway resistance (*6*, *7*). Binding of a muscle agonist, like histamine or acetylcholine, to a surface receptor on the SMC and the subsequent rise in cytosolic Ca^{2+} concentration, is the universal trigger for force generation in the smooth muscle (*8*). Agonist exposure induces Ca^{2+} oscillations in SMCs that propagate as waves within the smooth muscle layer (*9*). These agonist-induced Ca^{2+} oscillations serve two critical functions in the smooth muscle: (A) The concentration/dose of agonist detected by the surface receptors is transduced into the frequency of Ca^{2+} oscillations, with a higher concentration of muscle agonist resulting in a higher frequency

of Ca^{2+} oscillations, which can then be detected by downstream Ca^{2+} sensors and translated into a dose-dependent increase in smooth muscle contractility (*6*, *10*). (B) Agonist-induced Ca^{2+} oscillations propagate as waves around the circumference of the organ and enable the synchronized contractions of SMCs necessary to constrict the airway/blood vessels (*9*). At present, little is known about the role of extracellular mechanical factors such as ECM stiffness in regulating agonist-induced Ca^{2+} oscillations and Ca^{2+} waves that can move across an SMC ensemble.

In this study, we report a collective phenomenon in clusters of human airway smooth muscle cells, where ECM stiffness alters the intercellular communication between cells in an SMC ensemble causing increased Ca^{2+} oscillation frequencies and synchronized Ca^{2+} oscillations. This altered Ca^{2+} response results in a relative force increase by SMCs on stiff substrates. We examined intercellular transport of Ca^{2+} in SMC cells and we show that contrary to current dogma, the physical mechanism that enables intercellular Ca^{2+} waves does not involve molecular transport across gap junctions or paracrine signaling through extracellular diffusion. Rather, this phenomenon appears to be driven by force-transfer among cells in the cluster. The collective response of SMCs to agonist could be a mechanism by which matrix remodeling can drive disease progression in asthma and hypertension.

Results

1. Matrix stiffness alters the Ca^{2+} response to agonist in multicellular clusters of SMCs, but not in isolated cells.

Modeling the SMC layer in 2D using micropatterning: To study the role of altered matrix stiffness on the frequency of Ca^{2+} oscillations, we used micropatterning to create a 2D approximation of the organization of SMCs seen in lung slices (Fig. 1A, S1A). The substrate

we use is NuSil (*11*), an optically clear, non-porous polydimethylsiloxane substrate whose Young's modulus, E, can be varied in the range 0.3 kPa-70 kPa (*11*). Based on measurements of ECM stiffness in healthy human airways, we set the ECM stiffness of healthy human airways to E=0.3 kPa (*12*). This matches the ECM stiffness of small airways (inner diameter <3 mm) which are known to collapse in asthma (*13*). With the onset of airway remodeling, collagen is deposited in the airways and the stiffness of the ECM increases (*1*). A substrate stiffness of E=13 kPa was used to mimic remodeled ECM. These ECM stiffness values are also representative of the two distinct regimes of mechanosensing seen in all adherent cells (*14*, *15*). Using a Ca^{2+} sensitive fluorescent dye (Fluo4-AM), we imaged and quantified the time period of Ca^{2+} oscillations in these SM rings plated on soft and stiff ECM. Images were recorded at a rate of 1 per second for 5 minutes following exposure to 10^{-5} M histamine. On soft ECM (E=0.3 kPa), exposure to histamine resulted in Ca^{2+} oscillations with a mean time period of 43.64±1.45 seconds (N=4, Fig. 1E). When the substrate stiffness was increased to E=13kPa, the same dose of agonist induced significantly faster oscillations with a mean time period of 22.79±2.42 seconds (N=4, t-test, P<0.001, Fig. 1E**)**. Therefore, at the *same* dose of agonist, stiff substrates resulted in a doubling of the cytosolic Ca^{2+} oscillation frequency in healthy smooth muscle cells.

<u>Interactions between ECM and isolated cells are insufficient to explain altered Ca^{2+} response:</u> To explain the role of matrix stiffness in regulating the Ca^{2+} response to a low dose of agonist, we first hypothesized that this phenomenon was linked to cell-matrix interactions at the level of the individual cell. With increased matrix stiffness, SMCs develop higher cytoskeletal prestress (*15*) opening stretch-activated Ca^{2+} channels (*16*) and potentially increasing the Ca^{2+} flux into the cell. To test this hypothesis, we cultured human airway SMCs at a low density such that individual cells were isolated, spaced at least 100 μm from each other (Fig. 1B, S1B). We first measured baseline traction (pre-agonist) stress

exerted by these isolated cells on the substrate to confirm that the baseline traction was significantly higher in isolated cells cultured on stiff, with a mean traction stress of 15.95±5.02 Pa (N=21), versus isolated cells cultured on soft substrates, with a mean traction stress of 6.98±1.68 Pa (N=16). The corresponding median stresses were 6.89 Pa on soft matrix and 16.00 Pa on stiff substrate (Mann-Whitney Rank Sum test, $P<0.001$). We then exposed these isolated SMCs to 10^{-5} M histamine and measured the time period of Ca^{2+} oscillations. Contrary to our expectations, ECM stiffness had no impact on the Ca^{2+} response of isolated SMCs to 10^{-5} M histamine (Fig. 1F). Cells cultured on the soft substrate had a mean period of 66.11±10.55 seconds (N=14) and those on the stiff matrix had a mean period of 65.73±11.48 seconds (N=12), which was not statistically significantly different (t-test, P=0.930). Therefore, despite the higher levels of prestress in individual cells, ECM stiffening has no impact on the agonist-induced Ca^{2+} frequency of isolated cells.

SMCs sense matrix as a collective and alter their Ca^{2+} response to agonist: To probe this phenomenon further, starting with the isolated SMCs (Fig. 1B), we increased the seeding density (Fig. 1C, S1C) until we had a confluent cluster of SMCs (Fig. 1D, S1D). At each seeding density, we measured the time period of Ca^{2+} oscillations for SMCs adhering to soft (E=0.3 kPa) and stiff (E=13 kPa) substrates in response to 10^{-5} M histamine (Fig. 1F-1H). Sparsely seeded cells (Fig. 1G) responded similarly to isolated cells (Fig. 1F), exhibiting no statistically significant difference between the agonist-induced Ca^{2+} oscillations on soft and stiff matrix (t-test, P=0.481). The mean time period of oscillations of sparse SMCs on the soft substrate was 51.74±8.11 seconds (N=4) and 55.63±6.48 seconds (N=4) on the stiff substrate (Fig. 1G). Confluent cells behaved like those patterned in a ring, with cells plated on stiffer substrate exhibiting a significantly higher frequency of Ca^{2+} oscillations in response to 10^{-5} M histamine. Confluent SMCs on soft matrix had a mean time period of 58.36±5.89 seconds (N=5), and the same healthy, confluent cells on stiff matrix had a mean

period of 35.03±1.03 seconds (N=7, Fig. 1H). The corresponding median time periods were 58.87 seconds on soft matrix and 35.11 seconds on stiff matrix (Mann-Whitney Rank Sum Test, P=0.003). These results suggest the existence of a collective phenomenon in smooth muscle cells, where clusters of confluent SMCs alter their agonist-induced Ca^{2+} oscillations in response to changes in matrix stiffness while isolated cells do not. In the supplementary information (Fig. S2), we include additional measurements made on two intermediate stiffnesses, E=0.6 kPa, E=3 kPa, and glass (E→∞). These experiments confirm that Ca^{2+} oscillations resulting from exposure to 10^{-5} M histamine are unaffected by ECM stiffness in isolated SMCs, whereas in confluent cells, the same dose of agonist can evoke a significantly different Ca^{2+} response in SMCs depending on the stiffness of the underlying matrix. This finding is extremely significant in all smooth muscle pathologies because all downstream Ca^{2+} dependent molecular processes rely on Ca^{2+} oscillations to perceive the external concentration of contractile agonist detected by the G-protein coupled receptors on the cell surface. Here we show that the combination of confluence and ECM stiffness can alter how cells perceive contractile agonist.

2. Matrix stiffening synchronizes Ca^{2+} oscillations within a multicellular SMC cluster.

We next explored the nature of intercellular communication underlying the collective agonist-induced Ca^{2+} response in SMCs. To do this, we first analyzed the time series of histamine-induced Ca^{2+} oscillations for signs of interactions among the different SMCs within a confluent cluster. After correcting for drift due to photobleaching of the fluorophore, we calculated the cross-correlation coefficient ($\rho_{i,j} \in [-1,1]$) of the Ca^{2+} oscillations occurring in the i^{th} cell and the j^{th} cell in the cluster for all the cells in a cluster. The measured values of $\rho_{i,j}$ in a typical SMC cluster is depicted in Fig. 2A as a representative 24x24 matrix, with the extreme values $\rho_{i,j} \rightarrow 1$ (pink) indicating that the Ca^{2+} levels in the

i^{th} and j^{th} cell rise and fall perfectly in sync with each other (perfectly correlated) (Fig. 2B), $\rho_{i,j} \rightarrow$-1 (green) indicating that when the Ca^{2+} levels in i^{th} cell rises, the Ca^{2+} levels in the j^{th} cell falls and vice-versa (anti-correlated), $\rho_{i,j} \rightarrow 0$ (white) indicating no correlation in the Ca^{2+} oscillations occurring in i^{th} and j^{th} cells (Fig. 2B). To avoid the effects of histamine diffusion, the first 60 seconds immediately after application of histamine was not considered in the correlation calculation. Histograms of $\rho_{i,j}$ measured in isolated SMCs and confluent clusters of SMCs cultured on soft and stiff matrices are shown in Figs. 2C and 2D, respectively. Isolated SMCs (Fig. 2C), did not exhibit correlated Ca^{2+} oscillations, with a mean ρ of zero, regardless of whether they were cultured on soft (0.01±0.06, N=5) or stiff (0.03±0.06, N=4) substrates. However, for cells in a confluent cluster, matrix stiffening caused a statistically significant shift in ρ towards positive correlation (Fig. 2D). The mean ρ for confluent clusters on soft matrices was 0.03±0.04, N=4, versus on stiff matrices, ρ increased to 0.26±0.10, N=5. A two-way ANOVA test with confluence and ECM stiffness as independent factors showed a significant interaction between confluence and ECM stiffness (P=0.007). Post-hoc pairwise comparisons using the Holm-Sidak test showed a significant difference in the pairwise correlations in confluent clusters due to ECM stiffness (P<0.001). In the isolated cells, there was no statistical difference in the pairwise correlations due to ECM stiffness (P=0.733). We also did not observe any systematic relationship between the pairwise correlation in Ca^{2+} oscillations and the distance between the SMCs.

Next, we investigated the time it takes after the addition of histamine for the Ca^{2+} oscillations to synchronize. In order to do this, we repeated the previous calculation of cross-correlations, but instead of using the entire time series, we used a time window of 120 seconds starting at t=60 seconds after addition of histamine and repeated the $\rho_{i,j}$ calculation for the Ca^{2+} time series within this 120 seconds window for all cells in the cluster. The time

window was then shifted in increments of 15 seconds over the rest of the 5-minute time frame over which we measured Ca^{2+} oscillations. Shown in Fig. 2E and Fig. 2F are the average through time, $\rho_{i,j}(\tau)$ of cross-correlation coefficients between all cells either isolated or confluent, soft and stiff matrix, respectively. A two-way ANOVA with time after addition of histamine and ECM stiffness as the two independent factors shows no difference due to stiffness (P=0.303) or time (P=0.274) in isolated cells. However, in confluent cells on stiff ECM, the correlation coefficients gradually increase over time, for about 1 minute, which matches the time course for force generation in airway SMCs (*17*). In conjunction with our findings from the previous section, these results demonstrate that not only does the combination of a stiff matrix and confluent clusters of cells lead to faster Ca^{2+} oscillations, but it also causes histamine-induced Ca^{2+} oscillations to synchronize across the cells in the cluster.

3. Gap junctions do not play a role in regulating the collective Ca^{2+} response of SMC clusters.

The most well studied long-range communication mechanism in multicellular systems is the intercellular waves of Ca^{2+} that are capable of propagating over distances much longer than a cell length through a regenerative Ca^{2+} induced Ca^{2+} release mechanism (*18*). This mode of communication is mediated through two critical pathways: (i) gap junction channels, which connect the cytoplasm of neighboring cells and allow for the transport of signaling molecules from one cell to its neighbor and (ii) extracellular diffusion of a signaling molecule like ATP, which can diffuse and bind to purinergic receptors on neighboring cells, causing Ca^{2+} release in these cells (*19*).

Transport through gap junctions is unaffected by ECM stiffness: We first fluorescently labeled gap junctions by staining for connexin-43 (Cx43). The expression of Cx43 (red) for

confluent clusters of SMCs on soft and stiff substrates are shown in Figs. 3A and 3B, respectively. The actin filaments (green) and the nucleus (blue) are also labeled. From these images, we quantified the number of gap junctions per cell for confluent cells plated on soft and stiff substrates. There was no significant difference between Cx43 expression on soft and stiff substrates from N=5 independent samples per stiffness, each containing approximately 35 cell measurements (t-test, P=0.977) (Fig. 3C). Next, we tested whether ECM stiffness induced a change in the efficiency of transport through gap junctions. To this end, we employed a commonly used technique to quantitatively assess the efficiency of transport through gap junctions called gap-FRAP (*20*). Briefly, a confluent layer of SMCs was incubated with membrane-permeable calcein-AM. Upon entering the cell, the acetyl methyl ester bond was hydrolyzed by intracellular esterases, trapping the hydrophilic calcein molecule within the cell (Fig. 3D, column 1). The calcein in one cell selected at random was then bleached using a high-intensity laser (Fig. 3D, column 2). The bleached calcein molecules and the unbleached calcein molecules in neighboring cells diffuse through gap junctions leading to a recovery in fluorescence (Fig. 3D, column 3). The kinetics and extent of recovery in fluorescence in the bleached cell reflects the efficiency of transport across gap junctions via diffusion. A typical recovery curve is shown in Fig. 3E, where F_0, F_b, F_r indicate the fluorescence intensity in the target cell at baseline, after bleaching and after recovery. To quantify the extent of recovery, we calculated the mobile fraction, Γ, given by

$$\Gamma = \frac{F_r - F_b}{F_0 - F_b} \times 100\% \quad (1)$$

for confluent SMCs cultured on soft and stiff matrices (N=16, N=18 independent trials, respectively). We found no difference in the mobile fraction due to ECM stiffness. SMCs on soft matrix had a mean mobile fraction, Γ of 42.19±10.50%, and those on stiff matrix

had a Γ of 40.05±9.18% (t-test, P=0.532) (Fig. 3F). We also did not observe any statistically significant difference in the rate of recovery in fluorescence k_r, which was calculated by fitting an exponential function $F(t) = F_b + F_r(1-e^{-k_r t})$ to the recovery curve. On soft ECM, k_r was 0.01±0.02 (N=16) and on stiff ECM, k_r was 0.01±0.05 (N=18). There was no statistical difference in the rate of recovery due to ECM stiffness (t-test, P=0.55).

Blocking gap junctions does not affect agonist-induced Ca^{2+} oscillations: To further explore the role of gap junctions in the collective response of the SMCs to agonist, we used 30 μM of 18 β-glycyrrhetinic acid (βGA) to block transport across gap junctions. βGA causes dephosphorylation of connexins and disassembly of gap junctions (*21*). We first used gap-FRAP to verify that a 30 μM dose of βGA was sufficient to completely block transport across gap junctions. The mobile fraction, Γ, measured in a confluent layer of SMCs after application of 30 μM βGA dropped significantly from a mean of 40.05±9.18% to 6.84±2.89% (N=18, with corresponding medians 40.41% and 7.02%, respectively, Mann-Whitney Rank Sum Test, P<0.001) (Fig. 3F). This recovery is similar to the 7.89% recovery we measured in an isolated cell. Similar minimal recovery has been noted in the literature (*22*), indicating that transport across gap junctions was blocked. After 30 minutes of incubation with 30 μM dose of βGA, we measured histamine-induced Ca^{2+} oscillations in confluent clusters of SMCs. Much to our surprise, we found that blocking gap junctional transport had no impact on the histamine-induced Ca^{2+} oscillation periods in multicellular clusters of SMCs, regardless of the stiffness of the ECM (N=6 soft, N=4 stiff) (Fig. 3G). A two-way ANOVA with treatment (βGA) and ECM stiffness as the two independent factors showed no difference in the time period of histamine-induced Ca^{2+} oscillations due to treatment (P=0.784) for a given stiffness. Post-hoc pairwise comparisons with the Holm-Sidak method showed the Ca^{2+} oscillations remained significantly faster on the stiff matrix (P<0.001) even after blocking gap junctions.

4. Mechanical force transfer among cells regulates the collective Ca^{2+} response of SMC clusters.

Ca^{2+} wave propagation follows the contractile axis of the SMCs: Next, we considered extracellular diffusion of signaling molecules, such as ATP, as a possible mode of intercellular communication that enables the collective Ca^{2+} response of SMC clusters on stiff matrices (*18*). In order to do this, we measured the direction in which the Ca^{2+} wave propagates from one cell to the next in SMC clusters cultured on stiff substrates. If we select a cell in an SMC cluster, a wave that passes through it will appear as a localized increase in Ca^{2+} in the cell which is followed by a localized increase in Ca^{2+} in one of its neighbors. We reasoned that if the intercellular Ca^{2+} transport was being enabled by extracellular diffusion of signaling molecules, then the resulting Ca^{2+} wave should have an equal chance of moving in all directions (isotropic). We split the direction of propagation of the Ca^{2+} wave from an SMC into two directions: a direction parallel to the contractile axis of the SMC, and a direction perpendicular to the contractile axis of the SMC. For the cell labeled 1 shown in Fig. 4A (insets), cells 2 and 4 were considered parallel to cell 1's contractile axis and cells 3 and 5 were considered perpendicular to cell 1's contractile axis. We calculated the conditional probability for a localized increase in Ca^{2+} in one cell to be followed by a localized increase in a parallel neighbor versus its perpendicular neighbor. This conditional probability quantifies the isotropy in Ca^{2+} wave propagation with respect to the contractile axis of the SMC, with equal probability (0.5) in parallel and perpendicular direction indicating isotropy in Ca^{2+} wave propagation. Instead, we found that there was an 80.5±7.53% chance for the Ca^{2+} wave to follow the contractile axis of the SMC (Fig. 4B, N=10, t-test , $P<0.001$). The high probability of the Ca^{2+} wave to follow the contractile axis of the SMCs rules out extracellular diffusion as the dominant mechanism for intercellular communication in our experiments.

Mechanical force transfer between SMCs regulates their Ca^{2+} response: Thus far, we have ruled out transport through gap junctions and extracellular diffusion, the two widely accepted mechanisms responsible for intercellular communication in confluent cell clusters using Ca^{2+} waves (*18*). The propensity of Ca^{2+} waves to follow the direction of the contractile axis of the SMC suggested force transfer between neighboring SMCs as a potential mechanism that regulates the collective Ca^{2+} response of SMC clusters. To quantify SMC forces in our confluent clusters, we used Fourier transform traction force microscopy (*23*) to measure the traction stress generated by cells exposed to 10^{-5} M histamine. Traction stress is the force exerted by the cell normalized by the cross-sectional area over which the force acts. Before agonist stimulation, mean traction stresses for isolated cells were 6.98±1.68 Pa on soft (N=16) and 15.95±5.02 Pa on stiff (N=21) substrates, and 13.56±1.56 Pa on soft (N=12) and 14.26±1.89 Pa on stiff (N=21) for confluent cells. We found that histamine had generated a normalized traction (post-histamine traction stress/pre-histamine traction stress) of 1.22±0.11 in confluent cells on soft substrates (N=12). On stiffer matrix, a confluent cluster of SMCs from the same healthy donor and passage generated normalized force of 2.24±0.26 (N=21) (Fig. 4C). There was a statistically significant difference ($P<0.001$, t-test) between the force generated on soft and stiff substrates in response to the same dose of agonist. To test the possibility that higher force transfer among cells on stiff substrates was responsible for this collective phenomenon, we experimentally measured the effect of reducing muscle force on Ca^{2+} oscillations with two independent inhibitors of force generation: (1) Rho-associated kinase (ROCK) inhibitor, Y-27632, which reduces SMC force by inhibiting myosin light chain phosphorylation and by removing the inhibitory effect of ROCK on the activity of myosin light chain phosphatase and (2) myosin light chain kinase (MLCK) inhibitor, ML-7, which reduces force by inhibiting myosin light chain phosphorylation. Confluent SMC clusters on E=13 kPa matrix

were pre-treated with increasing doses of either Y-27632 for 1 hour prior to histamine exposure or increasing doses of ML-7 for 5 minutes prior to histamine exposure (Fig. 4D). We found that increasing the concentration of Y-27632 from 10 μM (N=3) to 100 μM (N=4) abolished the stiffness-induced reduction in time period of Ca^{2+} oscillations in a dose-dependent manner (One-Way ANOVA with treatment as the independent variable, $P<0.001$). Similarly, increasing the dose of ML-7 from 0.01 μM to 0.05 μM also abolished the stiffness-induced reduction in time period of Ca^{2+} oscillations in a dose-dependent manner (One-Way ANOVA, $P<0.001$). With both these inhibitors, the higher concentration resulted in histamine-induced Ca^{2+} oscillation periods on stiff matrices that were not statistically different from the histamine-induced Ca^{2+} oscillation periods on soft matrices. These results clearly demonstrate that the exaggerated histamine-induced Ca^{2+} response due to matrix stiffening can be *systematically*, and *completely* abrogated by reducing mechanical forces in the multicellular ensemble.

5. Confining the SMCs to a line reduces the variability in Ca^{2+} oscillation periods:

Comparing the alignment of SMCs in Fig. 1B to Fig. 1D and Fig. 4A, we observed that with the onset of confluence, SMCs naturally tend to organize themselves into spatial clusters of aligned cells. To test the effect of SMC alignment on the higher frequency of Ca^{2+} oscillation on stiff substrates, we compared the time period of Ca^{2+} oscillations in confluent SMC clusters to the time period of Ca^{2+} oscillations in SMC clusters micropatterned in a line which was 1000 μm long and 15 μm wide (~1 cell wide and ~10 cell lengths long) (Fig. 5A, S1E). The idea here was to eliminate the possibility of intercellular communication occurring perpendicular to the contractile axis in confluent clusters; through mechanisms that are less likely to be influenced by force. We found that while the mean time period of oscillations was nearly identical in both confluent SMC clusters and lines of SMCs, the

probability of cells with a higher time period of Ca^{2+} oscillations decreases when SMCs are aligned (Fig. 5B). An F-test shows a significant decrease in the variability of the time period distribution when the cells are aligned in a line (N=8 soft, N=6 stiff, P<0.001). This result is consistent with the idea that higher Ca^{2+} frequencies are being driven by force transfer along the contractile axis.

The effect of localized ECM stiffening can be sensed by SMCs over long distances: ECM remodeling in airways and blood vessels often occur as spatially localized processes. How does this pathological change in the ECM spread? Current theories require cells to migrate into the region of stiffer ECM for them to sense the altered matrix and respond by excessive secretion of matrix proteins thereby creating a positive feedback loop that leads to more ECM remodeling (*24*). However, given the collective nature of ECM stiffness sensing in SMC clusters, it may be possible for SMCs located far away from the site of ECM remodeling to detect this localized change, even though these SMCs are not physically in contact with the stiff ECM. To test this hypothesis and to quantify the distance over which a localized increase in ECM stiffness would be felt by an ensemble of SMCs, we created a dual-stiffness substrate (Fig. 5C), where the region marked in green has Young's modulus of 13 kPa and the region in black has Young's modulus of 0.3 kPa. We then patterned SMCs in a line starting from the stiff region and extending into the soft region. Cells on soft and stiff ECM were simultaneously exposed to 10^{-5} M histamine, and we measured the time period of Ca^{2+} oscillations in SMCs on the soft ECM for 5 minutes. The change in Ca^{2+} oscillation time period was not sudden as one moved from the stiff to the soft ECM (Fig. 5D). Rather, the mean time period increased at a slow rate of 1.83 s/100 μm. We grouped the cells by distance from the edge into 400 μm bins and statistically tested the difference in the time period of Ca^{2+} oscillations between each bin and cells in physical contact with the stiff substrate. We found that there was no statistically significant difference between

histamine-induced Ca^{2+} oscillations for cells on stiff substrates and cells up to 800 μm (approximately 8 cell lengths) away from the edge (N=4, Mann-Whitney Rank Sum Test, P=0.140). Cells beyond 800 μm had significantly different time periods (N=4, t-test, P<0.001). This result demonstrates that spatially localized alterations in the ECM can be detected by SMCs far from the site of ECM remodeling, suggesting that ECM pathology can spread through the organ much faster than currently believed.

Discussion

Increased stiffness of the extracellular matrix (ECM) that surrounds and supports cells in tissue is associated with a number of disease conditions ranging from cancer and fibrosis (*25*) to cardiovascular (*26*), lung (*1*), eye (*27*), and age-related diseases (*28*). Traditionally, pathological alterations in the ECM were thought to be the consequence of disease progression. However, it is now becoming increasingly apparent in many diseases that matrix stiffening precedes disease development and could, therefore, contribute to disease progression (*5*, *29*). Recognizing the importance of ECM remodeling, clinical trials were undertaken to restore the healthy, homeostatic state of the ECM (*30*). These early efforts were unsuccessful (*31*) and attention has now turned to understanding and targeting the mechanisms by which cells perceive and respond to changes in the ECM (*29*).

Here, we demonstrate a collective phenomenon in smooth muscle cells (SMC) in which matrix stiffness alters the intercellular communication between cells in an ensemble resulting in elevated contractility at low doses of agonist. We show that this collective mechanosensing phenomenon is enabled by crosstalk among cells using Ca^{2+} waves (*18*). A common mechanism of communication involves the molecular transport of Ca^{2+} and inositol trisphosphate (IP_3) across gap junctions. However, our measurements showed no tendency for molecular transport through gap junctions to differ depending on ECM

stiffness. We blocked transport through gap junctions using 18 β-glycyrrhetinic acid (βGA) (*32*) and confirmed that the dose we used was sufficient to completely disrupt molecular transport across gap junctions. Contrary to our expectations based on current models (*18*), blocking transport through gap junctions had no impact on the collective agonist response of SMCs to ECM stiffening. There was no change in the Ca^{2+} oscillation for SMCs on soft and stiff substrates after βGA treatment. Following a recent finding that mechanical forces can synchronize contraction of cardiac myocytes in the developing heart independent of gap junctions (*32*), we tested whether ECM stiffening led to a switch in the mode of communication between cells from molecular signaling through gap junctions to mechanical force based signaling.

Ca^{2+} waves can travel distances far greater than a cell length because Ca^{2+} waves regenerate in each cell by "calcium-induced calcium release" from the endoplasmic reticulum (ER). In the most widely accepted theory of long-range Ca^{2+} transport, Ca^{2+} release from the ER is enabled by a messenger molecule, IP_3, which diffuses faster than Ca^{2+} and activates the receptors on the ER, so when the Ca^{2+} wave arrives, it can release more Ca^{2+}. This theory had its basis in measurements of IP_3 diffusivity in the Xenopus extract model of the cytoplasm (*33*), which put the diffusivity of IP_3 at 400 $\mu m^2/s$ and that of Ca^{2+} at 40 $\mu m^2/s$. However, more recent measurements made in human cells show that IP_3 diffuses at a slower rate than Ca^{2+} (*34*). Our finding that molecular diffusion through gap junctions is not necessary to sustain Ca^{2+} waves in SMC clusters is consistent with the challenge to the dogma of Ca^{2+} wave propagation through gap junctions.

In contrast to Ca^{2+} wave propagation in other cell types, measurements in confluent SMC clusters (Fig. 4A,B) show that Ca^{2+} waves follow the direction of the contractile axis of the SMCs. Further, reducing the SMC force in our experiments with two independently-acting

muscle relaxants slowed the Ca^{2+} oscillations and intercellular Ca^{2+} waves (Fig. 4D), suggesting that mechanical force transfer from one cell to its neighbor enables the intercellular Ca^{2+} transport. Can force transfer between cells also serve as a mechanism that amplifies and modulates the frequency of oscillations as the Ca^{2+} wave moves from cell-to-cell? The mechanisms that underlie the findings of the present study can be understood in light of previous work from Felix et al (*35*) and Tanaka et al (*36*) who show that forces applied to a cell membrane cause PIP_2 to be hydrolyzed resulting in an increase in cytosolic IP_3 concentration. This would mean that for every SMC cell within a confluent cluster, there are two ways by which IP_3 can be released into the cytosol: (i) from agonist binding to GPCR receptors on the cell surface. (ii) from IP_3 generated by a contracting SMC pulling on its neighbor causing IP_3 release in the neighboring cell (*35*, *36*). This *additional* method of IP_3 release only exists for cells in a confluent cluster. Further, we have previously shown that force transfer between SMCs increases 8-fold with matrix stiffening (*12*). Such a force-based IP_3 release mechanism can explain how SMC clusters alter their agonist-induced Ca^{2+} oscillations in a matrix stiffness-dependent manner while isolated cells, which lack the second source of IP_3, do not.

Dysfunction in the smooth muscle has long been thought to be responsible for the exaggerated narrowing of transport organs like as asthma, hypertension and Crohn's disease. Asthma is an example of a disease where remodeling of the ECM is well characterized (*1*), but its effects are not considered in therapy or drug development. Asthmatics can be free of inflammation, and have spirometry and respiratory mechanics within the range of healthy individuals, up until they are exposed to a smooth muscle agonist at which point airways in an asthmatic will hyper-constrict (*37*). This exaggerated response of the airway is currently thought to result from the sensitization of force-generating pathways in the SMC due to prolonged exposure to inflammatory agents. Here, we

418 demonstrate that the fault may instead lie in changes in ECM stiffness that can regulate how
419 smooth muscle cells perceive agonist dose. To assess the overall magnitude and potential
420 physiological impact of the observed effect, we measured the Ca^{2+} response to different
421 doses of histamine at two different stiffnesses (Fig. S3). The data shows that if the ECM
422 stiffness of small airways (inner diameter<3 mm) in a healthy human lung with E=0.3 kPa
423 (*12*) were to remodel and become stiff (E=13 kPa), healthy airway SMCs would now
424 responds to a dose of 10^{-5} M histamine as though they received 10^{-3} M histamine (two log
425 dose higher concentration). We also demonstrate that the corresponding agonist-induced
426 force is also substantially higher (Fig. 4C).

427 There are several confounding factors to consider as one extrapolates these findings at the
428 length scale of cells to the length scale of the airway/lung. These confounding factors
429 include, but are not limited to (i) connectivity among smooth muscle cells within the airway:
430 to constrict an airway, SM cells need to connect with each other to form a percolating force
431 transfer path that winds around the circumference of the airway, and generates a force
432 sufficient to narrow the airway lumen. These physical connections between cells can occur
433 through direct cell-cell (cadherin-based contacts) or cell-ECM (focal adhesion) connections,
434 which are in turn dependent on mechanical forces (*12*). (ii) Transmural pressure: the
435 mechanical load presented by the ECM which will vary depending on the size of the airway
436 and the transmural pressure. (iii) Additional confounding factors: surface tension, airway
437 tone, parenchymal tethering forces, etc. will also play a role in dictating the degree to which
438 airway lumen narrows in response to smooth muscle activation by inhaled agonist.
439 Experimentally validating these results in lung tissue will require the development of new
440 technology to alter ECM stiffness of airways. With careful calibration, it might be possible
441 to adapt methods from tissue engineering like UV-induced crosslinking of collagen to study
442 the effects of ECM stiffening *in situ* in precision-cut lung slices.

443 At first glance, it appears contradictory that stretch decreases airway smooth muscle force
444 (*38*). Yet, stretch has also been shown to trigger a rise in cytosolic Ca^{2+} (*39*). The key to this
445 apparent paradox may be found in the single stretch experiments of Krishnan et al (*40*) as
446 well as computational models of the effect of stretch on muscle force (*15*). These studies
447 show that the decline in force occurs almost instantly upon stretching and is related to
448 rupture events in the cytoskeleton. The recovery, however, is slow and occurs at a timescale
449 of the order of 100s in human smooth muscle. When a cell is being subjected to cyclic
450 stretch (such as the length oscillations), the cell is attempting to recover its original prestress
451 which it lost immediately after the onset of stretch. To regain prestress, myosin activity is
452 required, and this necessitates higher Ca^{2+} levels.

453 ECM remodeling in airways and blood vessels often occur as spatially localized processes.
454 We also show that a spatially localized change in the ECM might be sufficient for
455 exaggerated force generation in SMCs far away from the site of ECM remodeling.
456 Consequently, the effects of ECM remodeling may manifest much earlier in disease
457 progression than currently believed. Our findings are relevant to discovering new pathways
458 by which ECM remodeling can be the primary driver of disease and for ongoing efforts to
459 develop new drugs that target mechanosensory pathways (*29*). For airway smooth muscle,
460 and asthma, in particular, these results show that the current treatment regimen may need to
461 shift to new paradigms that target matrix remodeling and mechanosensory pathways for a
462 more lasting cure.

463 **Materials and Methods**

464 **Fabrication of optically clear substrates of tunable stiffness:** NuSil is an optically clear,
465 biologically inert PDMS substrate with Young's Modulus tunable in the range from 0.3 kPa
466 to 70 kPa (*11*). Equal parts of NuSil gel-8100 parts A and B (NuSil, Carpinteria, CA, USA)

were mixed with various amounts of the crosslinking compound of Sylgard 184 (Dow Corning, Midland, MI, USA) to adjust substrate stiffness. A crosslinker volume 0.36% of the combined parts A and B volume was added for substrates with Young's modulus E= 13 kPa, and no crosslinker was added to the 1:1 A:B mixture for substrates with Young's modulus E= 0.3 kPa. After mixing, the substrate was spin coated onto 30 mm diameter, #1.5 glass coverslips for 50 seconds to produce a 100 µm-thick layer. They settled on a level surface at room temperature for 1 hour before curing at 60° C overnight. These cured substrates on coverslips were secured in sterile 40 mm Bioptech dishes (Biological Optical Technologies, Butler, PA, USA) to be used for cell culture.

Matrix protein coating: In order to coat the entire silicone substrate with protein, a volume of 0.1% gelatin solution was added and incubated at room temperature in the biosafety cabinet for 1 hour. To create protein patterns, we utilized the Alvéole's PRIMO optical module and the Leonardo software, a UV-based, contactless photopatterning system (Alvéole, Paris, France). The substrate surface was first coated with 500 µg/mL PLL (Sigma Aldrich, St. Louis, MO, USA) for 1 hour at room temperature. The substrate was washed with PBS and 10 mM HEPES buffer adjusted to pH 8.0, and then incubated with 50 mg/mL mPEG-SVA (Laysan Bio, Inc., Arab, AL, USA) at room temperature for 1 hour, and washed with PBS once more. The PRIMO system was calibrated using fluorescent highlighter on an identical substrate. The PBS was replaced by 14.5 mg/mL PLPP (Alvéole, Paris, France), and then the desired pattern, previously created with graphic software, was illuminated with UV light focused on the substrate surface for 30 seconds. Patterned surfaces were washed again with PBS and then incubated with 0.1% gelatin for 1 hour at room temperature. The substrate was washed and maintained hydrated in PBS at 4° C overnight.

Human airway smooth muscle cell culture: Primary human airway smooth muscle cells (SMCs) were acquired through the Gift of Hope foundation (via Dr. Julian Solway, M.D.,

University of Chicago) and through ATCC (https://www.atcc.org). Both these sources are public and pertinent medical information about the donor was relayed to us, but all donor identifiers are removed. The donor remains anonymous and cannot be identified directly or through identifiers linked to the subjects, meeting NIH guidelines. In this study, we used 4 healthy human donors with no history of asthma: 2 male, ages 59 and 34, and 2 female, ages 18 and 82. This study was carried out in accordance with the guidelines and regulations approved by the Institutional Biosafety Committee at Northeastern University. Cells were grown under standard culture conditions of 37º C and 5% CO_2 and utilized by P6 for all experiments. Culture medium: Cells were cultured in 10% fetal bovine serum, DMEM/F12 (Fisher Scientific), 1x penicillin/streptomycin (Fisher Scientific), 1x MEM non-essential amino acid solution (Sigma Aldrich), and 25 µg/L Amphotericin B (Sigma Aldrich). Prior to any measurements, the growth medium was switched to serum-free media for at least 24 hours. The serum-free medium was comprised of Ham's F-12 media (Sigma Aldrich), 1x penicillin/streptomycin, 50 µg/L Amphotericin B, 1x glutamine (Fisher Scientific), 1.7 mM $CaCl_2$ $2H_2O$, 1x Insulin-Transferrin-Selenium Growth Supplement (Corning Life Sciences; Tewksbury, MA), and 12 mM NaOH. Both patterned and non-patterned gelatin-coated substrates were UV sterilized for 1 hour, then incubated at 37° C for 1 hour before seeding human airway SMCs, passage 3-6. For patterned substrates, cells were seeded in Bioptech dishes at 10^4 cells per cm^2 and incubated for 10 minutes in 10% serum media to allow cells to adhere to patterns. Next, the dishes were washed with PBS to remove excess cells, and then filled with 10% serum media and incubated for 6 to 24 hours. For non-patterned substrates, cells were seeded at the desired density and then incubated in 10% serum media for 6 to 24 hours. After this time, media was replaced with serum-free media and incubated for at least 24 hours prior to measurements. For isolated cells, the seeding density was 10^2

cells per cm^2. For sparse cells, the seeding density was 10^3 cells per cm^2. For confluent cells, the seeding density was 10^4 cells per cm^2.

Fluorescent imaging of Ca^{2+}: Serum-starved airway SMCs were loaded with a fluorescent cytosolic Ca^{2+} indicator to record changes in [Ca^{2+}]. FLIPR Ca^{2+} 6 (Molecular Devices, San Jose, CA, USA) was used for all Ca^{2+} measurements except Fig. 1A, S1A, where we used Fluo4-AM (Sigma Aldrich, St. Louis, MO, USA). The commonly used Fluo4-AM is prone to photobleaching, and the measured Ca^{2+} traces must be bleach-corrected prior to measurements of the time period. FLIPR Ca^{2+} 6, on the other hand, did not photobleach even after 30 minutes of continuous imaging at 1 Hz. Fluo4-AM was prepared according to the manufacturer's standards. Cells were loaded with 0.2 μM Fluo4-AM solution, diluted in HBSS, and incubated at room temperature for 1 hour. Next, the cells were washed with HBSS and incubated in the dark in HBSS for an additional 30 minutes. The cells were washed once more before imaging. FLIPR Ca^{2+} 6 was also prepared according to manufacturer's standards. Cells were incubated with a 1:1 solution of FLIPR Ca^{2+} 6 and serum-free media at 37° C and 5% CO_2 for 2 hours before imaging. Both Ca^{2+} indicators use acetoxymethyl esters to pass through the cell membrane, which are then hydrolyzed by cytosolic esterases, trapping the fluorescent dye inside the cell. Cells were imaged with a Leica DMi8 inverted microscope, a Leica DFC6000 camera (Leica, Wetzlar, Germany), and a Lumencor Sola SEII LED light source (Lumencor, Beaverton, OR, USA). A FITC filter cube (excitation: 480/40 nm, emission: 527/50 nm) was used to image the fluorescent dye. Fluorescent intensity increases with increasing cytosolic [Ca^{2+}]. 16-bit images were recorded at 1 Hz for 1 minute before agonist addition, and for at least 5 minutes after 10^{-5} M histamine exposure. In order to analyze data, each image sequence was loaded in Fiji ImageJ, and regions of interest (ROIs) were hand-selected in the cytoplasm of each cell to obtain mean grayscale intensities over the area of the ROI for each frame in time. A custom

MATLAB (MathWorks, Natick, MA, USA) code was written to process the data and measure mean Ca^{2+} oscillation periods. This code measured mean Ca^{2+} oscillation periods by finding peaks in the time series data above a certain prominence and taking the mean of the time between all sequential peaks (Fig. S4).

Cell traction force measurements: The base NuSil substrates were coated with a layer of fluorescent beads as fiducial markers for traction force microscopy. A 5% solution of 0.2 μm diameter red fluorescent carboxylate-modified microspheres (FluoSpheres, Invitrogen, Carlsbad, CA, USA) in PBS was vortexed for 10 seconds. 2 mL of solution was added to each substrate in a Bioptech dish and left at room temperature for 1 hour to allow the beads to adhere. The bead solution was poured off, substrates were washed 3x with PBS, and then PBS was poured off. NuSil solution was prepared as described before, with the appropriate amount of crosslinker to match the stiffness of the base substrate. NuSil was spin-coated onto the newly bead-coated base substrate at 2500 RPM to create a 1 μm-thick layer and seal the beads. These substrates rested on a flat surface for 1 hour before curing overnight at 60° C. Substrates were protein-coated and seeded with cells as before. After a 24 hour incubation in serum-free media, the SMC tractions were recorded by imaging the fluorescent beads with a 20x/0.55 dry objective and the Leica DMi8 microscope in an environmental chamber maintained humidified at 37° C. Images were taken at baseline, after a 15 minute incubation with 10^{-5} M histamine, and after cells were removed using RLT Lysis Buffer (Qiagen, Hilden, Germany). Using these images, cellular forces were calculated with a custom MATLAB (MathWorks, Natick, MA) software program using Fourier Traction Force Microscopy (*23*).

Fluorescent labeling of connexin-43/actin/nuclei: Cells were fluorescently labeled for connexin-43 (Cx43) and filamentous actin (F-actin). Cells were fixed in 4% paraformaldehyde in PBS at room temperature for 10 minutes. Then, cells were

permeabilized with 100% ethanol for 10 minutes at 20° C. Following permeabilization, cells were blocked using 1x PBS containing 0.1% Tween-20, 1% bovine serum albumin (BSA), and 22.52 mg/ml glycine for 30 minutes at room temperature. Next, cells were stained for Cx43 (ab11370; Abcam, Cambridge, UK) at a dilution of 1:200 in 1x PBS containing 1% BSA for 1 hour at 37° C. Secondary antibody labeling and phalloidin staining were done simultaneously at dilutions of 1:200 and 1:40, respectively, using Alexa Fluor 594 (ab150080; Abcam, Cambridge, UK) and Alexa Fluor 488 Phalloidin (A12379; Invitrogen, Carlsbad, CA, USA). Lastly, cells were labeled with NucBlue (Fisher Scientific, Waltham, MA, USA) to label cell nuclei. Images were acquired using a 63x/1.4 oil-immersion objective (Leica, Wetzlar, Germany).

The gap-FRAP assay: Gap Fluorescent Recovery After Photobleaching (FRAP) is an experimental technique that has been established as an effective method of observing gap-junctional communication of small fluorescent molecules between adjacent cells (*22*). SMCs were cultured on NuSil gels of E=0.3 kPa and E=13 kPa until confluence was achieved, and then serum-starved for at least 24 hours prior to the experiment. Cells were loaded with 1 μM calcein-AM solution diluted in warmed 1x PBS solution and incubated at 37° C and 5% CO_2 for 15 minutes. Calcein-AM is a cell-permeable dye that is hydrolyzed into fluorescent calcein by cytoplasmic esterases upon entry through cell membrane and has been shown to permeate through gap junctions due to its low molecular size (622 Da) (*20*). After dye incubation, samples were washed with warm 1x PBS solution and returned to serum-free medium for experiments. FRAP was performed using a ZEISS confocal laser scanning microscope system equipped with a 20x/0.8 objective and a 488 nm Argon laser. Fluorescence data was captured using ZEN 2012 SP5 imaging software (ZEISS, Oberkochen, Germany). Samples were placed in an incubation chamber maintaining 37° C during experiments to preserve cell viability during imaging. Prior to photobleaching, a

manual ROI was drawn around the border of a target cell visibly connected to adjacent cells. Whole cells were selected for photobleaching to ensure that fluorescence recovery could only be attributed to the diffusion of calcein from adjacent cells. Laser power was adjusted to 1% and images were acquired every 5 seconds for 50 seconds using scan speed 12 (pixel dwell = 0.42 μs) to provide baseline fluorescence measurements. After baseline scans were acquired, the laser power was adjusted to 100% and cells were bleached to at least 20% of their initial fluorescence using scan speed 2 (pixel dwell = 40 μs). Following the bleaching step, fluorescence recovery images were collected every 5 seconds for approximately 5 mins at 1% laser power. The images from gap-FRAP experiments were analyzed using Fiji ImageJ software. First, baseline fluorescence intensities from the target cell were averaged over the first 10 frames captured to establish a reference value for fluorescence recovery. Next, fluorescence intensities were measured during the recovery period and divided by the average baseline intensity to normalize the data. To account for any photobleaching occurring during the recovery period, fluorescence intensities were collected from a region at the edge of the field of view. These values were used to adjust the intensity of the target cell over time to account for fluorescence degradation due to repeated scanning of the microscopic field, since the edge region was not affected directly during the bleaching step. The normalized fluorescence values of the bleached cell during recovery were plotted as a function of time. To compare fluorescence recovery across multiple sample groups, the mobile fraction of fluorescent molecules was calculated. Mobile fraction (Γ) measures the fraction of fluorescent molecules that contribute to recovery of fluorescence in bleached cells and is calculated with Eq. 1, where F_0, F_b, F_r indicate the fluorescence intensity in the cell being bleached at baseline, after bleaching and after recovery, respectively (Fig. 3E).

Gap junction blocker experiments: Gap junctions between confluent SMCs were blocked with 18β-glycyrrhetinic acid (βGA) (Sigma Aldrich, St. Louis, MO, USA). Confluent SMCs

on soft (E=0.3 kPa) and stiff (E=13 kPa) substrates were incubated with 30 μM βGA at 37° C and 5% CO_2 for 30 minutes. Although βGA is a common gap junction blocker, it has been reported to affect cell viability at higher concentrations (*21*). We used gap-FRAP to find the lowest possible dose of βGA that still blocked gap junctions between confluent cells, which we used here in our experiments. This treatment was used in conjunction with the Ca^{2+} imaging protocol to investigate the role of gap junctional diffusion in agonist-induced Ca^{2+} oscillations.

Force-inhibitor experiments: Smooth muscle cell contractile force was reduced with two separate inhibitors of force: Y-27362 (Sigma Aldrich, St. Louis, MO, USA), a specific inhibitor of ROCK, and ML-7 (Sigma Aldrich, St. Louis, MO, USA), a selective inhibitor of MLCK. Confluent SMCs on soft (0.3 kPa) and stiff (13 kPa) substrates were pre-incubated with 10 μM or 100 μM of Y-27632 for 1 hour, or 0.01 μM or 0.05 μM of ML-7 for 5 minutes, in tandem with the 2 hour FLIPR Ca^{2+} 6 indicator incubation, before experiments. Ca^{2+} imaging and 10^{-5} M histamine addition was added as previously described.

Data presentation and statistical testing: Throughout the manuscript, we represent data as the average of N independent trials. The error bars indicate standard deviation over independent trials. The individual data points are shown in all bar plots. Each data point is in turn the average of measurements made over multiple cells within one trial. Sigmastat (Systat Software, San Jose, CA) was used to perform statistical tests. Two-Way ANOVAs followed by posthoc pairwise comparisons were used to test for significant differences in datasets which were influenced by two independent factors. One-Way ANOVAs followed by posthoc pairwise comparisons were used to test for significant differences in datasets of three or more groups which were influenced by one independent factor. Pairwise comparisons used the t-test when the data was normally distributed. Otherwise, the Mann-

Whitney Rank Sum Test was used to compare the median values. The specific tests used, the number of samples and the P-value are described along with the corresponding results. A P-value of 0.05 was used as the threshold for a statistically significant difference between data sets.

References and Notes

1. B. B. Araujo, M. Dolhnikoff, L. F. F. Silva, J. Elliot, J. H. N. Lindeman, D. S. Ferreira, A. Mulder, H. A. P. Gomes, S. M. Fernezlian, A. James, T. Mauad, Extracellular matrix components and regulators in the airway smooth muscle in asthma. *Eur. Respir. J. Off. J. Eur. Soc. Clin. Respir. Physiol.* **32**, 61–9 (2008).
2. A. L. James, J. G. Elliot, R. L. Jones, M. L. Carroll, T. Mauad, T. R. Bai, M. J. Abramson, K. O. McKay, F. H. Green, Airway smooth muscle hypertrophy and hyperplasia in asthma. *Am. J. Respir. Crit. Care Med.* **185**, 1058–1064 (2012).
3. R. Saunders, H. Kaul, R. Berair, S. Gonem, A. Singapuri, A. J. Sutcliffe, L. Chachi, M. S. Biddle, D. Kaur, M. Bourne, I. D. Pavord, A. J. Wardlaw, S. H. Siddiqui, R. A. Kay, B. S. Brook, R. H. Smallwood, C. E. Brightling, DP2 antagonism reduces airway smooth muscle mass in asthma by decreasing eosinophilia and myofibroblast recruitment. *Sci. Transl. Med.* **11**, eaao6451 (2019).
4. B. C. Berk, K. Fujiwara, S. Lehoux, ECM remodeling in hypertensive heart disease. *J. Clin. Invest.* **117**, 568–75 (2007).
5. T. Thenappan, S. Y. Chan, E. K. Weir, Role of extracellular matrix in the pathogenesis of pulmonary arterial hypertension. *Am. J. Physiol. Heart Circ. Physiol.* **315**, H1322–H1331 (2018).
6. M. J. Sanderson, P. Delmotte, Y. Bai, J. F. Perez-Zogbhi, Regulation of airway smooth muscle cell contractility by Ca2+ signaling and sensitivity. *Proc. Am. Thorac. Soc.* **5**, 23–31 (2008).

7. Y. S. Prakash, M. S. Kannan, G. C. Sieck, Regulation of intracellular calcium oscillations in porcine tracheal smooth muscle cells. *Am. J. Physiol.* **272**, C966-75 (1997).

8. D. C. Hill-Eubanks, M. E. Werner, T. J. Heppner, M. T. Nelson, Calcium signaling in smooth muscle. *Cold Spring Harb. Perspect. Biol.* **3**, a004549 (2011).

9. J. F. Perez, M. J. Sanderson, The frequency of calcium oscillations induced by 5-HT, ACH, and KCl determine the contraction of smooth muscle cells of intrapulmonary bronchioles. *J. Gen. Physiol.* **125**, 535–553 (2005).

10. A. B. Parekh, Decoding cytosolic Ca2+ oscillations. *Trends Biochem. Sci.* **36**, 78–87 (2011).

11. H. Yoshie, N. Koushki, R. Kaviani, M. Tabatabaei, K. Rajendran, Q. Dang, A. Husain, S. Yao, C. Li, J. K. Sullivan, M. Saint-Geniez, R. Krishnan, A. J. Ehrlicher, Traction Force Screening Enabled by Compliant PDMS Elastomers. *Biophys. J.* **114**, 2194–2199 (2018).

12. S. R. Polio, S. E. Stasiak, R. R. Jamieson, J. L. Balestrini, R. Krishnan, H. Parameswaran, Extracellular matrix stiffness regulates human airway smooth muscle contraction by altering the cell-cell coupling. *Sci. Rep.* **9**, 9564 (2019).

13. N. T. Tgavalekos, M. Tawhai, R. S. Harris, G. Musch, G. Mush, M. Vidal-Melo, J. G. Venegas, K. R. Lutchen, Identifying airways responsible for heterogeneous ventilation and mechanical dysfunction in asthma: an image functional modeling approach. *J. Appl. Physiol.* **99**, 2388–2397 (2005).

14. D. Mitrossilis, J. Fouchard, A. Guiroy, N. Desprat, N. Rodriguez, B. Fabry, A. Asnacios, Single-cell response to stiffness exhibits muscle-like behavior. *Proc. Natl. Acad. Sci.* **106**, 18243–18248 (2009).

15. H. Parameswaran, K. R. Lutchen, B. Suki, A computational model of the response of adherent cells to stretch and changes in substrate stiffness. *J. Appl. Physiol.* **116**, 825–834 (2014).

16. M. T. Kirber, J. V Walsh, J. J. Singer, Stretch-activated ion channels in smooth muscle: a mechanism for the initiation of stretch-induced contraction. *Pflugers Arch.* **412**, 339–45 (1988).

17. S. S. An, B. Fabry, X. Trepat, N. Wang, J. J. Fredberg, Do biophysical properties of the airway smooth muscle in culture predict airway hyperresponsiveness? *Am. J. Respir. Cell Mol. Biol.* **35**, 55–64 (2006).

18. L. Leybaert, M. J. Sanderson, Intercellular Ca(2+) waves: mechanisms and function. *Physiol. Rev.* **92**, 1359–92 (2012).

19. L. Leybaert, IP3, still on the move but now in the slow lane. *Sci. Signal.* **9**, fs17–fs17 (2016).

20. M. Abbaci, M. Barberi-Heyob, J. R. Stines, W. Blondel, D. Dumas, F. Guillemin, J. Didelon, Gap junctional intercellular communication capacity by gap-FRAP technique: A comparative study. *Biotechnol. J.* **2**, 50–61 (2007).

21. X. Guan, S. Wilson, K. K. Schlender, R. J. Ruch, Gap-junction disassembly and connexin 43 dephosphorylation induced by 18β-glycyrrhetinic acid. *Mol. Carcinog.* **16**, 157–164 (1996).

22. M. Kuzma-Kuzniarska, C. Yapp, T. W. Pearson-Jones, A. K. Jones, P. A. Hulley, Functional assessment of gap junctions in monolayer and three-dimensional cultures of human tendon cells using fluorescence recovery after photobleaching. *J. Biomed. Opt.* **19**, 015001 (2014).

23. J. P. Butler, I. M. Tolić-Nørrelykke, B. Fabry, J. J. Fredberg, Traction fields, moments, and strain energy that cells exert on their surroundings. *Am. J. Physiol. Cell Physiol.* **282**, C595-605 (2002).

24. F. Liu, J. D. Mih, B. S. Shea, A. T. Kho, A. S. Sharif, A. M. Tager, D. J. Tschumperlin, Feedback amplification of fibrosis through matrix stiffening and COX-2 suppression. *J.*

716 *Cell Biol.* **190**, 693–706 (2010).
717 25. T. R. Cox, J. T. Erler, Remodeling and homeostasis of the extracellular matrix:
718 implications for fibrotic diseases and cancer. *Dis. Model. Mech.* **4**, 165–78 (2011).
719 26. A. M. Briones, S. M. Arribas, M. Salaices, Role of extracellular matrix in vascular
720 remodeling of hypertension. *Curr. Opin. Nephrol. Hypertens.* **19**, 187–94 (2010).
721 27. A. R. Harper, J. A. Summers, The dynamic sclera: extracellular matrix remodeling in
722 normal ocular growth and myopia development. *Exp. Eye Res.* **133**, 100–11 (2015).
723 28. J. M. Phillip, I. Aifuwa, J. Walston, D. Wirtz, The Mechanobiology of Aging. *Annu. Rev.*
724 *Biomed. Eng.* **17**, 113–141 (2015).
725 29. M. C. Lampi, C. A. Reinhart-King, Targeting extracellular matrix stiffness to attenuate
726 disease: From molecular mechanisms to clinical trials. *Sci. Transl. Med.* (2018),
727 doi:10.1126/scitranslmed.aao0475.
728 30. J. A. Sparano, P. Bernardo, P. Stephenson, W. J. Gradishar, J. N. Ingle, S. Zucker, N. E.
729 Davidson, Randomized Phase III Trial of Marimastat Versus Placebo in Patients With
730 Metastatic Breast Cancer Who Have Responding or Stable Disease After First-Line
731 Chemotherapy: Eastern Cooperative Oncology Group Trial E2196. *J. Clin. Oncol.* **22**,
732 4683–4690 (2004).
733 31. A. Winer, S. Adams, P. Mignatti, Matrix Metalloproteinase Inhibitors in Cancer Therapy:
734 Turning Past Failures Into Future Successes. *Mol. Cancer Ther.* **17**, 1147–1155 (2018).
735 32. K. K. Chiou, J. W. Rocks, C. Yingxian, S. Cho, K. E. Merkus, A. Rajaratnam, C. Y. Chen,
736 S. Cho, K. E. Merkus, A. Rajaratnam, P. Robison, M. Tewari, K. Vogel, S. F. Majkut, B.
737 L. Prosser, D. E. Discher, A. J. Liu, Mechanical signaling coordinates the embryonic
738 heartbeat. *Proc. Natl. Acad. Sci. U. S. A.* **113**, 8939–44 (2016).
739 33. N. L. Allbritton, T. Meyer, L. Stryer, Range of messenger action of calcium ion and
740 inositol 1,4,5-triphosphate. *Science (80-.).* **258**, 1812-1815 (1992).

741 34. G. D. Dickinson, K. L. Ellefsen, S. P. Dawson, J. E. Pearson, I. Parker, Hindered
742 cytoplasmic diffusion of inositol trisphosphate restricts its cellular range of action. *Sci.*
743 *Signal.* **9**, ra108–ra108 (2016).
744 35. J. A. Felix, M. L. Woodruff, E. R. Dirksen, Stretch increases inositol 1,4,5-trisphosphate
745 concentration in airway epithelial cells. *Am. J. Respir. Cell Mol. Biol.* **14**, 296–301 (1996).
746 36. Y. Tanaka, S. Hata, H. Ishiro, K. Ishii, K. Nakayama, Quick stretch increases the
747 production of inositol 1,4,5-trisphosphate (IP3) in porcine coronary artery. *Life Sci.* **55**,
748 227–235 (1994).
749 37. S. S. An, T. R. Bai, J. H. T. Bates, J. L. Black, R. H. Brown, V. Brusasco, P. Chitano, L.
750 Deng, M. Dowell, D. H. Eidelman, B. Fabry, N. J. Fairbank, L. E. Ford, J. J. Fredberg, W.
751 T. Gerthoffer, S. H. Gilbert, R. Gosens, S. J. Gunst, A. J. Halayko, R. H. Ingram, C. G.
752 Irvin, A. L. James, L. J. Janssen, G. G. King, D. a Knight, A. M. Lauzon, O. J. Lakser, M.
753 S. Ludwig, K. R. Lutchen, G. N. Maksym, J. G. Martin, T. Mauad, B. E. McParland, S. M.
754 Mijailovich, H. W. Mitchell, R. W. Mitchell, W. Mitzner, T. M. Murphy, P. D. Paré, R.
755 Pellegrino, M. J. Sanderson, R. R. Schellenberg, C. Y. Seow, P. S. P. Silveira, P. G. Smith,
756 J. Solway, N. L. Stephens, P. J. Sterk, a G. Stewart, D. D. Tang, R. S. Tepper, T. Tran, L.
757 Wang, Airway smooth muscle dynamics: a common pathway of airway obstruction in
758 asthma. *Eur. Respir. J. Off. J. Eur. Soc. Clin. Respir. Physiol.* **29**, 834–60 (2007).
759 38. J. J. Fredberg, D. Inouye, B. Miller, M. Nathan, S. Jafari, S. H. Raboudi, J. P. Butler, S. A.
760 Shore, Airway smooth muscle, tidal stretches, and dynamically determined contractile
761 states. *Am. J. Respir. Crit. Care Med.* **156**, 1752–1759 (1997).
762 39. H. R. W. Wirtz, L. G. Dobbs, Calcium Mobilization and Exocytosis After One Mechanical
763 Stretch of Lung Epithelial Cells. *Science (80-.).* **250**, 1266–1269 (1990).
764 40. R. Krishnan, C. Y. Park, Y. C. Lin, J. Mead, R. T. Jaspers, X. Trepat, G. Lenormand, D.
765 Tambe, A. V. Smolensky, A. H. Knoll, J. P. Butler, J. J. Fredberg, Reinforcement versus

fluidization in cytoskeletal mechanoresponsiveness. *PLoS One*. **4** (2009), doi:10.1371/journal.pone.0005486.

Acknowledgments: Funding: This work was supported by NIH grants HL129468 and HL122513 (HP) and GM110268 (EJC). **Author contributions:** SS & HP conceived the idea and designed the experiments. With few exceptions, all experimental measurements and data analysis were performed by SS. RR and JB performed the gap-FRAP experiments. RR also performed the gap junction staining. SS, RR, JB, EJC & HP contributed to writing the manuscript and analysis of the data. HP is the corresponding author who conceived and directed this project.

Competing interests: The authors declare that they have no competing interests.

Data and materials availability: Data supporting the findings of this study are available within the manuscript. All other relevant data are available from authors upon reasonable request.

Figures and Tables

Fig. 1. Effect of matrix stiffness on agonist-induced Ca^{2+} oscillations in SMCs. (**A**) To study the role of altered matrix stiffness on the time period of agonist-induced Ca^{2+} oscillations, we micropatterned a 2D approximation of the in-situ organization of SMCs. Cells were also cultured on non-patterned surfaces in three different densities: (**B**) isolated, (**C**) sparse, and (**D**) confluent. The colors in Figs 1A-D correspond to cytosolic [Ca^{2+}] concentrations as indicated by the color bar in Fig. 1A. Scale bars=200 μm. (**E**) Increasing matrix stiffness from 0.3 kPa to 13 kPa caused a significant decrease in Ca^{2+} oscillation period in SMCs rings (t-test, $P<0.001$, N=4 each). (**F, G**) The periods of SMC Ca^{2+} oscillations were not affected

by matrix stiffness in both isolated (soft N=14, stiff N=12) and sparse (N=4 each) conditions (t-test, P=0.93, P=0.481, respectively). (**H**) Confluent cells behaved like those patterned in a ring, with cells plated on stiff matrix exhibiting significantly faster Ca^{2+} oscillations in response to 10^{-5} M histamine compared to those on a soft matrix (soft N=5, stiff N=7, Mann-Whitney Rank Sum Test, P=0.003). These results demonstrate that matrix stiffness can modulate the agonist-induced Ca^{2+} response of confluent SMCs, but not that of isolated cells.

Fig. 2. Effect of matrix stiffness and confluence on the correlated nature of Ca^{2+} oscillations. (**A**) The cross-correlation coefficients ($\rho_{i,j}$) range in values from 1 (positively correlated, pink) to 0 (uncorrelated, white) to -1 (negatively correlated, green), as shown in a representative 24x24 cell matrix. (**B**) Examples of Ca^{2+} oscillations measured in two cells with high pairwise-correlation (ρ=0.78), and low pairwise correlation (ρ=0.02). (**C**) In isolated cells, the Ca^{2+} oscillations were generally uncorrelated with a probability density function centered around zero. ECM stiffness did not affect pairwise correlations in isolated SMCs (N=5 soft, N=4 stiff, P=0.733, Two-Way ANOVA). (**D**) In confluent cells, there is a statistically significant increase in ρ, indicating that the Ca^{2+} oscillations were more synchronized on stiffer ECM (N=4 soft, N=5 stiff, Two-Way ANOVA, P=0.007). (**E, F**) To evaluate the time it takes after agonist addition for Ca^{2+} oscillations to become synchronized, we calculated $\rho_{i,j}(\tau)$ within a 120s moving window. (**E**) $\rho_{i,j}(\tau)$ in isolated cells does not change over time (N=5 soft, N=4 stiff, P=0.274) or with stiffness (P=0.303) (Two-Way ANOVA). However, **(F)** in confluent cells on stiff matrix, $\rho_{i,j}(\tau)$ shows a significant increase after 30 seconds (N=4 soft, N=5 stiff) (Two-Way ANOVA, P<0.001). Error bars indicate standard deviation.

Fig. 3. Effect of matrix stiffness on intercellular communication via gap junctions. Confluent SMCs on soft (**A**) and stiff (**B**) matrix were stained for the gap junction protein Cx43, actin, and the nucleus. (**C**) Gap junctions were counted for each SMC in individual frames on soft (N=5) and stiff (N=5) matrix, represented by the mean and standard deviation of these measurements, and we found no statistical difference due to matrix stiffening (t-test, P=0.977). (**D**) Diffusion through gap junctions was quantified by bleaching a small fluorescent molecule within a cell and measuring signal recovery due to intercellular diffusion, a technique called gap-FRAP. (**E**) A representative recovery curve for one cell shows a recovery of ~40% its initial fluorescence. These values were used to calculate mobile fraction, a measure of diffusion efficiency through gap junctions. (**F**) Matrix stiffness had no effect on mobile fraction (t-test, soft N=16, stiff N=18, P=0.532). The gap junction blocker βGA significantly reduced the recovery (**D**) and mobile fraction (**F**) (N=18, Mann-Whitney Rank Sum Test). (**G**) Despite blocking gap junctions with βGA, there was no effect on Ca^{2+} oscillation periods in confluent cells on either soft (N=6) or stiff (N=4) matrix (Two-Way ANOVA, P=0.784 treatment within stiffness). Scale bars= 30 μm.

Fig. 4. Role of mechanical force in Ca^{2+} wave propagation through multicellular ensembles of SMCs. (**A**) SMCs in confluent layers form organized clusters of cells, with certain cells aligned end-to-end along their contractile axis (parallel), and others branching off at an angle (perpendicular). Scale bar=250 μm. Insets (**a**), (**b**) show cells 2 and 4 parallel to the contractile axis of cell 1, whereas cells 3 and 5 are perpendicular. Inset scale bars=50 μm. The conditional probability for a localized increase in Ca^{2+} in cell 1 to be followed by an increase in a parallel or perpendicular neighbor is plotted in (**B**) with mean and standard deviation. Ca^{2+} waves were

statistically more likely to propagate along the contractile axis (t-test, N=10). (**C**) Histamine caused a significantly greater increase in traction stress in confluent cells on stiff matrix (N=21) rather than on soft (N=12, t-test). (**D**) The faster agonist-induced Ca^{2+} oscillations on stiff ECM were systematically abrogated in a dose-dependent manner by preincubating the SMCs with the ROCK inhibitor Y-27632 for 1 hour prior to histamine exposure (N=3, N=4, $P<0.001$, One-Way ANOVA). Identical results can be obtained with MLCK inhibition by preincubating with increasing doses of ML-7 for 5 minutes (N=3 each, $P<0.001$, One-Way ANOVA).

Fig. 5. Effect of confining SMCs in a line using micropatterning. (**A**) When SMCs were patterned in lines, (**B**) the probability of finding SMCs with high time periods decreased and the variance of the time periods from aligned cells was significantly smaller than confluent cells (F-test, $P<0.001$). Matrix stiffness still affected the oscillation period (soft N=8, stiff N=6, Mann-Whitney Rank Sum Test). To probe the limits of the SMC cluster's collective matrix sensing abilities, we simulated localized ECM stiffening by (**C**) patterning SMCs in lines spanning a dual-stiffness PDMS substrate (E=13 kPa highlighted in green, left, and E=0.3 kPa, right). (**D**) The Ca^{2+} oscillation time period of cells along lines is plotted as a function of the distance from the stiff matrix. Binning cells in 400 μm intervals, only those over 800 μm from stiff matrix had different Ca^{2+} oscillation time periods from cells directly in contact (t-test, N=4). **S**cale bars=250 μm.

Supplementary Materials

Materials and Methods

Fabrication of NuSil substrates at additional stiffnesses: Equal parts of NuSil gel-8100 parts A and B (NuSil, Carpinteria, CA, USA) were mixed with various amounts of the crosslinking compound of Sylgard 184 (Dow Corning, Midland, MI, USA) to adjust substrate stiffness. Crosslinker volumes of 0.07% and 0.15% of the combined volumes of parts A and B were added to the 1:1 A:B mixture to create substrates with Young's modulus E= 0.6 kPa and 3 kPa, respectively. The spinning and curing protocol to finish the substrates can be found in the main manuscript.

Histamine dose-response experiment: Confluent SMCs cultured on soft (0.3 kPa) and stiff (13 kPa) substrates were incubated with FLIPR Ca^{2+} 6 indicator and imaged following the protocol in the main manuscript. For each sample, histamine concentration was gradually increased and followed by 5 minutes of imaging. Stiff samples were exposed to concentrations increasing from 10^{-6} M, to 10^{-5} M, to 10^{-4} M, and soft samples were exposed to concentrations of 10^{-5} M, 10^{-4} M, and 10^{-3} M histamine.

Figures

Fig. S1.

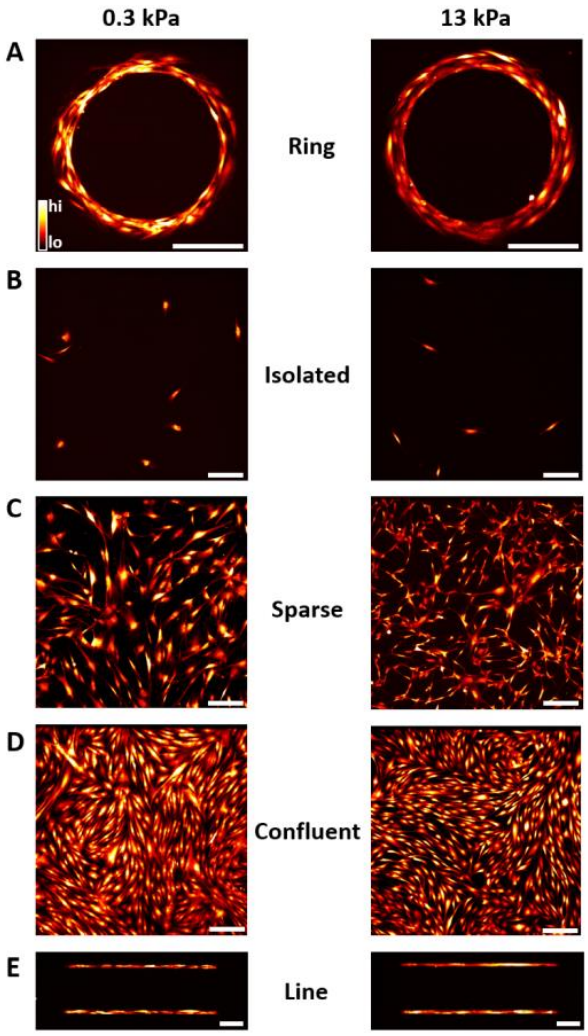

Fig. S1. Morphology of SMCs on soft and stiff substrates. Fluorescent images of cytosolic Ca^{2+} in SMCs show similar appearance and density of cells in the different culture conditions used in this paper: (**A**) rings, (**B**) isolated, (**C**) sparse, (**D**) confluent, and (**E**) lines. The cytosolic [Ca^{2+}] is pseudo-colored following the color bar, as in Fig. 1. Scale bar = 200 μm.

Fig. S2.

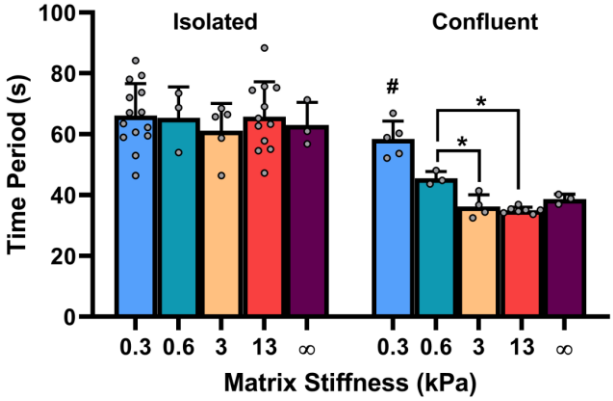

Fig. S2. Effect of incremental matrix stiffening on agonist-induced Ca^{2+} oscillations in SMCs. PDMS substrate stiffness was tuned between our limits for soft (0.3 kPa) and stiff (13 kPa) matrix to create two intermediate stiffness matrices at 0.6 kPa and 3 kPa. Glass coverslips were used to represent matrix of infinite stiffness. In confluent cells, ECM stiffness had a significant impact on agonist-induced Ca^{2+} oscillation time periods (One-Way ANOVA, $P<0.001$). Pairwise comparisons with a Holm-Sidak test are indicated by symbols. The time period at 0.3 kPa was significantly different from all other substrate stiffnesses (indicated by #, $P<0.001$). The time period at 0.6 kPa was also significantly different from that at 3 kPa and 13 kPa ($P=0.003$, $P<0.001$, respectively). There was no statistical difference between time periods at 3 kPa, 13 kPa and glass (3 kPa vs. 13 kPa $P=0.566$, 3 kPa vs. glass $P=0.379$, 13 kPa vs. glass $P=0.017$, respectively). Matrix stiffness had no effect on the agonist-induced Ca^{2+} response in isolated cells (One-Way ANOVA, $P=0.907$).

Fig. S3.

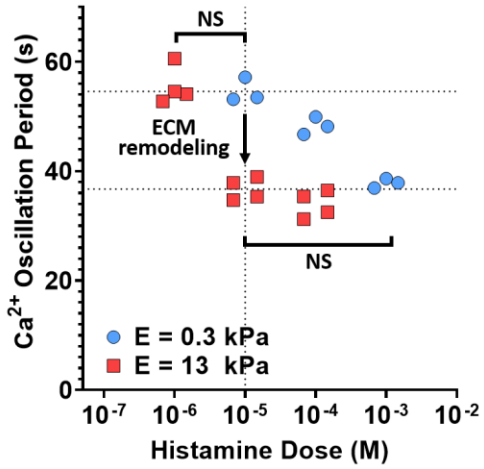

Fig. S3. Effect of histamine dose on Ca^{2+} oscillation time period for cells on soft and stiff ECM. Confluent SMCs on soft and stiff matrix were exposed to multiple doses of histamine. Increasing concentration of histamine from 10^{-5} M to 10^{-3} M systematically decreased the mean Ca^{2+} oscillation time periods of cells on soft matrix (One-Way ANOVA, $P<0.005$). On stiff matrix, increasing histamine dose from 10^{-6} M to 10^{-5} M caused a dramatic decrease in time period, but increasing the dose further had no effect (One-Way ANOVA, $P<0.001$, $P=0.174$, respectively). For SMCs on soft ($E=0.3$ kPa) substrate, the histamine dose needs to be increased from 10^{-5} M to 10^{-3} M (2 log scales higher) to match the Ca^{2+} response of SMCs on the stiff substrate.

Fig. S4.

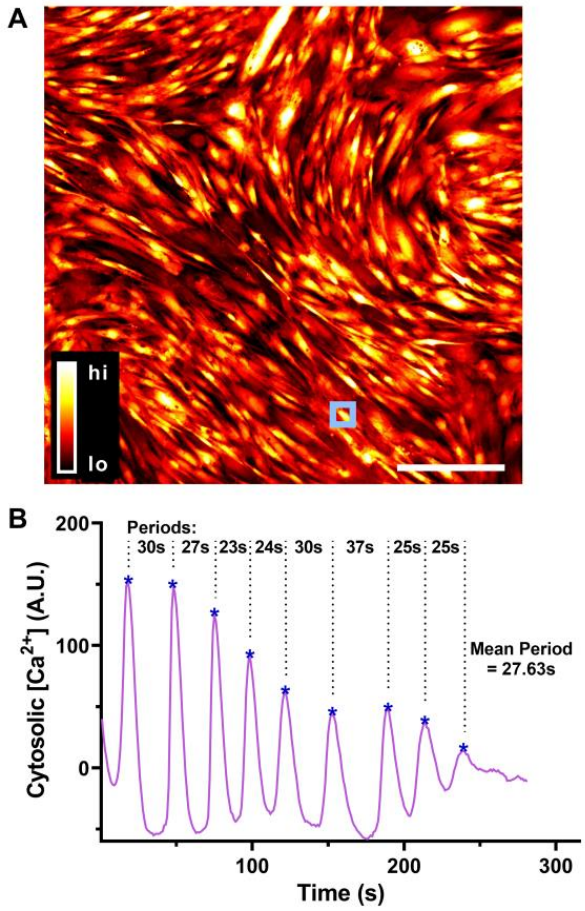

Fig. S4. Method of calculating Ca^{2+} oscillation periods. (**A**) Images for each experiment were loaded into Image J, and 5x5 pixel regions of interest (ROIs) were hand-selected in the cytosol of the smooth muscle cell. The mean gray intensity of each ROI for each frame was imported into MATLAB and plotted to show changes over time for each cell. The Ca^{2+} indicator used in our experiments indicates cytosolic $[Ca^{2+}]$, therefore changes in grayscale intensity correspond with changes in cytosolic $[Ca^{2+}]$. (**B**) The portion of data after the initial spike in Ca^{2+} due to histamine addition was selected for further processing. First, the code subtracted the mean $[Ca^{2+}]$ value of each time series from the time series. Next, local peaks above a threshold value were identified (indicated by *), and the time between sequential peaks were recorded as oscillation periods. Time

periods are measured for a minimum of 40 cells/trial in confluent cells and for every SMC in isolated cells. The average time period of all measured cells is reported for each independent trial.

Movies S1 to S4 Captions

Movie S1. Cytosolic Ca^{2+} oscillations in confluent smooth muscle cells on stiff matrix. Confluent SMCs on stiff matrix (E=13 kPa) loaded with a fluorescent Ca^{2+} indicator were imaged before and during exposure to a 10^{-5} M dose of the contractile agonist histamine, added at the time indicated. This movie shows the first 2.5 minutes of the experiment. The movie is compressed to 8 bit and 0.25 frames/second to match journal data guidelines. The full 5 minutes of Ca^{2+} oscillations recorded at 1 frame/second, 16-bit, 2048 x 2048 images used to make measurements is available from the authors on reasonable request. Scale bar = 200 μm.

Movie S2. Cytosolic Ca^{2+} oscillations in confluent smooth muscle cells on soft matrix. Confluent SMCs on soft matrix (E=0.3 kPa) loaded with a fluorescent Ca^{2+} indicator were imaged before and during exposure to a 10^{-5} M dose of the contractile agonist histamine, added at the time indicated. This movie shows the first 2.5 minutes of the experiment. The movie is compressed to 8 bit and 0.25 frames/second to match journal data guidelines. The full 5 minutes of Ca^{2+} oscillations recorded at 1 frame/second, 16-bit, 2048 x 2048 images used to make measurements is available from the authors on reasonable request. Scale bar = 200 μm.

Movie S3. Cytosolic Ca^{2+} oscillations in isolated smooth muscle cells on stiff matrix. Isolated SMCs on stiff matrix (E=13 kPa) loaded with a fluorescent Ca^{2+} indicator were imaged before and during exposure to a 10^{-5} M dose of the contractile agonist histamine, added at the time indicated. This movie shows the first 2.5 minutes of the experiment. The movie is compressed to 8 bit and 0.25 frames/second to match journal data guidelines. The full 5 minutes of Ca^{2+} oscillations recorded at 1 frame/second, 16-bit, 2048 x 2048 images used to make measurements is available

from the authors on reasonable request. Scale bar = 200 μm.

Movie S4. Cytosolic Ca^{2+} oscillations in isolated smooth muscle cells on soft matrix. Isolated SMCs on soft matrix (E=0.3 kPa) loaded with a fluorescent Ca^{2+} indicator were imaged before and during exposure to a 10^{-5} M dose of the contractile agonist histamine, added at the time indicated. This movie shows the first 2.5 minutes of the experiment. The movie is compressed to 8 bit and 0.25 frames/second to match journal data guidelines. The full 5 minutes of Ca^{2+} oscillations recorded at 1 frame/second, 16-bit, 2048 x 2048 images used to make measurements is available from the authors on reasonable request. Scale bar = 200 μm.